GeroScience
https://doi.org/10.1007/s11357-020-00289-8

ORIGINAL ARTICLE

Whole brain irradiation in mice causes long-term impairment in astrocytic calcium signaling but preserves astrocyte-astrocyte coupling

Adam Institoris · Ciaran Murphy-Royal · Stefano Tarantini · Andriy Yabluchanskiy · Jordan N. Haidey · Anna Csiszar · Zoltan Ungvari · Grant R. Gordon

Received: 13 August 2020 / Accepted: 14 October 2020

Abstract Whole brain irradiation (WBI) therapy is an important treatment for brain metastases and potential microscopic malignancies. WBI promotes progressive cognitive dysfunction in over half of surviving patients, yet, the underlying mechanisms remain obscure. Astrocytes play critical roles in the regulation of neuronal activity, brain metabolism, and cerebral blood flow, and while neurons are considered radioresistant, astrocytes are sensitive to γ-irradiation. Hallmarks of astrocyte function are the ability to generate stimulus-induced intercellular Ca^{2+} signals and to move metabolic substrates through the connected astrocyte network. We tested the hypothesis that WBI-induced cognitive impairment associates with persistent impairment of astrocytic Ca^{2+} signaling and/or gap junctional coupling. Mice were subjected to a clinically relevant protocol of fractionated WBI, and 12 to 15 months after irradiation, we confirmed persistent cognitive impairment compared to controls. To test the integrity of astrocyte-to-astrocyte gap junctional coupling postWBI, astrocytes were loaded with Alexa-488-hydrazide by patch-based dye infusion, and the increase of fluorescence signal in neighboring astrocyte cell bodies was assessed with 2-photon microscopy in acute slices of the sensory-motor cortex. We found that WBI did not affect astrocyte-to-astrocyte gap junctional coupling. Astrocytic Ca^{2+} responses induced by bath administration of phenylephrine (detected with Rhod-2/AM) were also unaltered by WBI. However, an electrical stimulation protocol used in long-term potentiation (theta burst), revealed attenuated astrocyte Ca^{2+} responses in the astrocyte arbor and soma in WBI. Our data show that WBI causes a long-lasting decrement in synaptic-evoked astrocyte Ca^{2+} signals 12–15 months postirradiation, which may be an important contributor to cognitive decline seen after WBI.

Keywords WBI · WBRT · Whole brain radiation therapy · Aging · Cognitive impairment · Radiation · Dementia

A. Institoris · C. Murphy-Royal · J. N. Haidey · G. R. Gordon (✉)
Department of Physiology and Pharmacology, Cumming School of Medicine, Hotchkiss Brain Institute, University of Calgary, Calgary, Alberta, Canada
e-mail: gordong@ucalgary.ca

S. Tarantini · A. Yabluchanskiy · A. Csiszar · Z. Ungvari
Department of Biochemistry and Molecular Biology, Vascular Cognitive Impairment and Neurodegeneration Program, Reynolds Oklahoma Center on Aging/Oklahoma Center for Geroscience, University of Oklahoma Health Sciences Center, Oklahoma City, OK, USA

S. Tarantini · Z. Ungvari
International Training Program in Geroscience, Doctoral School of Basic and Translational Medicine/Department of Public Health, Semmelweis University, Budapest, Hungary

Introduction

Whole brain irradiation (WBI, also known as whole brain radiation therapy or WBRT) remains an important treatment option for patients with both identifiable brain metastases and as a prophylaxis for microscopic

Published online: 22 October 2020

malignancies [1, 2]. Incidence of brain involvement in patients with metastatic cancer is 10–40%. Over 200,000 cancer patients receive either partial large field or WBI every year in the USA for this indication [3]. Although WBI is clinically effective in eliminating proliferating cancer cells, there is a growing concern regarding serious unwanted side effects and late toxicity profile in brain tissue. WBI causes progressive impairments in verbal and spatial memory, attention, novel problem-solving ability, and executive function in over 50% of surviving patients, which manifests months to years after treatment, compromising quality of life [4–6]. WBI-induced cognitive impairment progresses to dementia in about 2 to 5% of long-term survivors [7]. WBI also leads to a progressive impairment of cognitive function in laboratory rodents [6, 8–12], modeling the full clinical picture. The mechanisms responsible for WBI-induced cognitive impairment remain obscure, and there are no effective treatments or prevention strategies.

Astrocytes are an abundant cell type in the brain and play critical roles in regulation of neuronal function and cerebral blood flow (CBF). While neurons are considered radioresistant [13], astrocytes are sensitive to γ-irradiation [12, 14, 15]. There is increasing preclinical evidence suggesting that the profound harmful effects of WBI on cognitive function are due, at least in part, to irradiation-induced phenotypic and functional changes in astrocytes [16]. Furthermore, there is prima facie evidence that irradiation-induced astrocytic alterations may promote neuronal excitotoxicity [15], compromise the essential role of astrocytes in regulation of regional CBF [12], and associate with impaired energy metabolism and blood-brain-barrier disruption [17].

An important measurement to assess astrocyte function as it relates to neuronal function is the generation and propagation of stimulus-induced intercellular Ca^{2+} transients and waves [18]. Increases of astrocytic cytosolic Ca^{2+} mediate many cellular events including gliotransmitter release from perisynaptic processes, as well as changes of the diameter of resistance vessels at perivascular endfeet by regulating the production/release of vasoactive mediators [19–26]. Importantly, astrocytes are coupled to each other via gap junctions forming an astrocytic syncytium, which allows localized Ca^{2+} signals to be spread to adjacent cells. This connectivity is also critical for the shuttling of metabolic substrates such as glucose and lactate to help fuel neuronal activity [27]. Preclinical studies show that neurodegeneration is associated with behaviorally relevant changes in astrocyte Ca^{2+} signaling [28]. Studies on transgenic animal models establish a causal link between compromised astrocytic Ca^{2+} signaling and cognitive and behavioral impairment [29–31]. In multiple excitable cell types, as well as in cultured astrocytes, γ-irradiation was shown to alter Ca^{2+} handling, expression of Ca^{2+} channels, endoplasmic reticulum function and/or gap junctional communication [32–34]. Despite these advances, the effects of WBI on astrocytic Ca^{2+} signaling and gap junctional coupling are unknown.

Using a clinically relevant irradiation protocol in mice, combined with 2-photon fluorescence assessments in acute cortical brain slices, we test the hypothesis that WBI-induced cognitive impairment associates with persistent impairment of astrocytic Ca^{2+} signaling and/or gap junctional coupling.

Materials and methods

Experimental animals and experimental design

To understand the effects of WBI on astrocyte Ca^{2+} signaling, we used mice from an existing cohort of WBI-treated transgenic p16-3MR mice [35]. These mice carry a trimodal fusion protein (3MR) under the control of the $p16^{Ink4a}$ promoter in a C57BL/6 background [36] and were used recently to detect senescent cells in the irradiated brain [12]. Two-month-old mice were housed 3 per cage in the specific pathogen free animal facility at the University of Oklahoma Health Sciences Center (OUHSC). Both male and female mice were used. Animals were kept on a 12-h light/dark cycle and fed standard rodent chow and water ad libitum, following standard husbandry techniques. One week before irradiation, mice were transferred to the conventional animal facility of the OUHSC and housed under similar conditions. Mice were anesthetized and subjected to WBI ($n = 23$, 5 Gy twice weekly for a total cumulative dose of 40 Gy) or sham-irradiated as a control group ($n = 16$). Mice were then left to recover in the original environment. Twelve months after the WBI protocol, mice were tested for cognitive function. A subgroup of this cohort was transferred to the University of Calgary for assessment of astrocytic Ca^{2+} signaling and of intercellular coupling. For astrocyte coupling experiments, naïve 13-month-old male mice were used ($n = 4$) as control.

All animal protocols were approved by the Institutional Animal Care and Use Committee of the University of Oklahoma Health Sciences Center and the University of Calgary.

Fractionated whole brain irradiation protocol

After acclimating to the conventional facility for 1 week, mice were randomly assigned to either control or irradiated groups. Animals were weighed and anesthetized via i.p. injection of ketamine and xylazine (100/15 mg per kg). Mice in the irradiated group were subjected to clinically relevant WBI (5 Gy twice weekly for a total cumulative dose of 40 Gy) as described [12]. Radiation was administered using a ^{137}Cesium gamma irradiator (GammaCell 40, Nordion International). A Cerrobend® shield was utilized to minimize exposure outside the brain. The radiation dose received by the mice was verified using film dosimetry, as described [11, 37].

Radial-arm water maze testing

To determine how WBI affects cognitive function, spatial memory and long-term memory were tested by assessing performance in the radial arms water maze at 12 months postWBI, following our published protocols [12]. The maze consists of 8 arms with a submerged escape platform at the end of one arm. Food coloring was added to the water to make it opaque. The maze was surrounded by privacy blinds with extramaze visual cues. Intramaze visual cues were placed at the end of the arms. Mice were monitored by video tracking directly above the maze, and parameters were measured using Ethovision software (Noldus Information Technology Inc., Leesburg, VA, USA). Experimenters were blinded to the experimental conditions of the mice. Each day, mice were given the opportunity to learn the location of the submerged platform during 2 session blocks, each consisting of 4 consecutive acquisition trials. On each trial, the mouse was started in an arm not containing the platform and allowed to wade for up to 1 min to find the escape platform. All mice spent 30 s on the platform following each trial before beginning the next trial. The platform was located in the same arm on each trial. Over 3 days of training, mice gradually improved performance. Upon entering an incorrect arm (all 4 paws within the distal half of the arm), the mouse was charged an error. Learning was assessed by comparing performance on days 2 and 3 of the learning period. When both groups learned the task, mice were placed in their home cage for 7 days. Then, they were given a recall trial on day 10 (probe day). On day 11 (extinction and reversal), mice were tested for ability to extinguish and relearn the task when the platform had been moved to a different arm not adjacent or diametrically positioned to the previous location. Mice were tested for 2 session blocks, extinction and reversal, both consisting of 4 trials.

Tissue collection, preparation of brain slices

Terminal experiments were conducted 12–15 months after irradiation similar to previously published protocols [27, 38, 39]. Mice were briefly anesthetized with isoflurane (5%) before decapitation. For astrocyte coupling experiments, mice were transcardially perfused with 5-ml ice-cold slicing solution (in mM as follows: 119.9 N-methyl-D-glucamine, 2.5 KCl, 25 $NaHCO_3$, 1.0 $CaCl_2$-$2H_2O$, 6.9 $MgCl_2$-$6H_2O$, 1.4 NaH_2PO_4-H_2O, and20 D-glucose)before sacrificing them. Coronal slices (300-μm thickness) of the sensory-motor cortex were acutely cut with a vibratome (Leica VT-1200S) and incubated in artificial cerebrospinal fluid (ACSF) saturated with 95% O_2/5% CO_2 for 45 min at 34 °C. ACSF contained (in mM): NaCl (126); KCl (2.5); $NaHCO_3$ (25); $CaCl_2$ (1.5); $MgCl_2$ (1.2); NaH_2PO_4 (1.25); and glucose (10). Imaging was performed at 22 °C, and slices were superfused at ~ 2 ml/min.

Assessment of astrocytic Ca^{2+} signaling

A custom-made two-photon microscope [40] equipped with a Zeiss 40x/1.00 NA 2.5 mm WD objective lens and a Chameleon Ultra Ti:Sapph laser (coherent) was used for imaging. Time series used a field size of 200–290 μm^2 at 1 Hz (512 pixels^2).

After the 45-min recovery, slices used for Ca^{2+} imaging were incubated for 45 min at 34 °C with the synthetic indicator rhodamine-2 acetoxymethyl ester (Rhod-2/AM, 15 μM, Biotium) in 0.2% DMSO; 0.006% pluronic acid; and 0.0002% Cremophore EL [39]. Astrocytes were identified by brighter fluorescence than neurons and the presence of endfeet apposed to the vasculature. Ca^{2+} signals from neuropil, astrocyte somata, and endfeet were outlined and analyzed using ImageJ (NIH) and Prism software (GraphPad Inc.) as $\Delta F/F = ((F_1–F_0)/F_0) \times 100$-100 [39].

Electrical brain slice stimulation and pharmacology

Cortical afferent stimulation was implemented by a Grass S88X stimulator, voltage-isolation unit, and a concentric bipolar electrode (FHC) positioned 200-μm lateral from the imaging area in layer 2/3 of the neocortex [38]. To elicit a Ca^{2+} transient in all astrocyte compartments, the tissue was stimulated with a long-term potentiation (LTP) protocol of theta burst pattern (100-Hz trains of 1 ms pulses for 50 ms, repeated at 4 Hz) for 30 s [38, 41–43]. Stimulation intensity was chosen by adding 0.1 V to the lowest stimulus intensity that elicited endfoot Ca^{2+} elevation at a shorter and lower frequency (5 s, 20 Hz) stimulation. Phenylephrine hydrochloride (10 μM, Tocris Biosciences) was topically superfused for 20 min while astrocytes were imaged 40-μm deep from the slice surface, in layers 1 and 2/3 of the neocortex.

Assessment of astrocyte coupling with patch-based dye infusion

Astrocyte coupling was assessed with patch-based dye infusion according to the published methods of Murphy-Royal et al. [27]. In brief, for coupling experiments, sulforhodamine-101 (SR-101, 10 μM, Sigma-Aldrich) was bulk loaded for 20 min immediately after slice recovery in an incubation chamber that was also bubbled with carbogen and then slices returned to their ACSF incubator for an hour to allow for the complete uptake and stabilization of the SR-101 signal.

The intracellular patch solution contained Alexa-488 sodium hydrazide (100–200 μM, Invitrogen) to visualize the diffusion of the patch solution throughout the network of astrocytes. Control intracellular solution contained the following (in mM): 108 potassium gluconate, 8 KCl, 8 sodium gluconate, 2 $MgCl_2$, 10 HEPES, 0.1 potassium EGTA, 4 ATP, and 0.3 sodium GTP. Internal solution was corrected for osmolarity to ~ 285 mosmol and corrected for pH with KOH to 7.2. A successful astrocyte patch was confirmed by a low input resistance (10–20 MΩ), dye transfer via gap junctions between coupled cells, and dye appearance in endfeet around microvessels. Astrocytes were voltage-clamped at − 85 mV. Tau (s), the time constant e^{-1} of the monoexponential fit to the dye filling curve, is the time it took Alexa-488-hydrazide to reach ~ 63% maximum brightness in coupled neighboring cell bodies was quantified and compared with an unpaired *t* test for each cell between the WBI and naïve groups.

qPCR: expression of glutamate receptors

We quantified mRNA expression of various metabotropic and ionotropic glutamate receptors by qPCR in WBI and control mice. Using validated TaqMan probes (Applied Biosystems) and a Strategen MX3000 platform, as previously reported [12]. Total RNA was isolated with a Mini RNA Isolation Kit (Zymo Research, Orange, CA) and was reverse transcribed using Superscript III RT (Invitrogen) as described previously [12]. Quantification was performed using the ΔΔCq method. The relative quantities of the reference genes *Hprt*, *Ywhaz*, *Gapdh*, *Hmbs*, *Polr2a*, *Actb*, and *S18* were determined and a normalization factor was calculated based on the geometric mean for internal normalization.

Statistical analysis

The normality of each data set was first assessed with a Shapiro–Wilk test. Normally distributed data were compared with unpaired *t* test, but where normality failed, Mann–Whitney *U* test was applied. The behavioral data were compared with unpaired *t* test. The tau value of neighboring astrocyte filling was compared with unpaired *t* test. We analyzed group differences in the peak astrocyte soma Ca^{2+} signals using generalized linear models in SPSS (IBM SPSS Statistics, Version 25). Nonresponding astrocytes, where the maximum fluorescence increase in response to stimulation was < 3 standard deviation of the 10-s prestimulus baseline, were excluded (6 cells in total). The target variable was the astrocyte soma Ca^{2+} peak, which was best fitted with a Gamma distribution, with log link. The size of initial neuronal process Ca^{2+} response of the neuropil was included as a continuous covariate. Fixed effects included main effect of WBI, and irradiation-by-size of initial neuronal process Ca^{2+} response interaction. Significance level for main effects and interactions was set at $p < 0.05$. *P* values for post hoc pairwise contrasts were automatically Bonferroni corrected in the model. All data are expressed as mean ± standard error of the mean.

Results

WBI impairs cognitive performance in mice

We assessed the effects of WBI on learning and memory in mice 12 months after WBI using the radial-arm water

maze (Fig. 1a) [12]. During acquisition, mice from both groups neither showed significant changes in the path length (not shown) nor in the combined error rate across days, indicating equal learning of the task. Combined error rates in control nonirradiated ($n = 12$) and WBI-treated mice ($n = 10$) were tallied on the retrieval day 10 (probe day) and during extinction and reversal. While we found no differences between control (errors = 1.7 ± 0.5) and WBI (errors = 2.0 ± 0.4) on the probe day ($P = 0.27$, Fig. 1b), WBI mice showed higher error counts compared to controls on both the extinction (errors = 6 ± 0.4 vs 4.2 ± 0.5, $P = 0.03$) (Fig. 1c) and reversal (errors = 5.8 ± 0.2 vs 3 ± 0.6, $P = 0.02$) (Fig. 1d) sessions (unpaired t tests). These data show that WBI mice can acquire spatial memory similar to controls, but exhibit enhanced extinction of memory, as well as deficits in cognitive flexibility 12-month postirradiation.

Astrocyte-to-astrocyte gap junctional coupling is unaffected by WBI

Astrocytes are coupled to each other via gap-junctions forming an astrocytic syncytium. The rapid distribution of small molecules and metabolic substrates along their concentration gradient through the interconnected network of astrocytes is essential for (1) synaptic plasticity by shuttling lactate to active synapses [27], (2) eliminating byproducts of synaptic activity (K^+, glutamate) [44, 45], and (3) modulating spatiotemporal dynamics of neuronal networks by allowing Ca^{2+} signals to propagate between remote synapses [46]. Hampered trafficking through interconnected astrocytes develops with acute stress and may be responsible for stress-induced amnesia [27]. Astrocyte uncoupling was also shown to contribute to early epileptogenesis [44, 47].

To test the integrity of astrocyte-to-astrocyte gap junctional coupling postWBI, we patch loaded individual cortical astrocytes with the Alexa-488-hydrazide and recorded the increase of fluorescence signal in neighboring astrocyte cell bodies with 2-photon microscopy (Fig. 2a). Fluorescent intensity in the patched astrocyte rose rapidly after whole-cell configuration was achieved (after rupturing a patch of cell membrane) and elevated slowly in adjacent astrocytes (Fig. 2b–d). We calculated the time constant (tau) of dye transfer to neighboring cells (Fig. 2e), which is unrelated to the tau of the patched cell [27] and independent of absolute fluorescence measures. Tau values in cells from WBI brains (tau = 186 ± 31 s; mean ± SEM, $n = 13$ cells, 7 slices, 4 mice) were not different from brains of nonirradiated naïve mice (tau = 169 ± 17 s; $n = 29$ cells, 16 slices, 4 mice, $P = 0.648$, Mann–Whitney U test, Fig. 2f), suggesting WBI had no long lasting impact on astrocyte-astrocyte coupling.

WBI elicits persistent alterations in astrocytic Ca^{2+} signaling

Increases of free Ca^{2+} in astrocytes mediate a plethora of cellular events, including gliotransmitter release onto synapses from fine astrocyte processes and release of vasoactive messengers onto microvasculature from

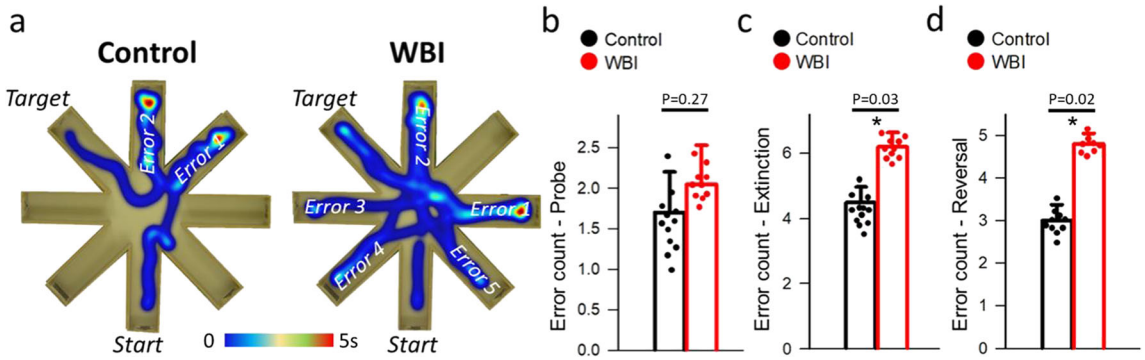

Fig. 1 Whole brain irradiation (WBI) impairs performance of mice in the radial-arm water maze (RAWM). Control ($n = 10$) and WBI treated mice ($n = 12$) were tested in the RAWM. **a** Heatmap representing the percentage of time spent in different locations in the maze for a randomly selected animal from each group during the reversal phase. Note that the WBI-treated mouse required more time and a longer path length in order to find the hidden escape platform than control animals. The WBI-treated mouse also reentered a previously visited arm multiple times. Combined error rates in control and WBI-treated mice on **b** the probe on day 10 and **c** during extinction and **d** reversal. Each data point represents the average of 4 to 8 independent trials for the same animal. All data are shown as mean ± SEM. Unpaired t test. *$P < 0.05$ vs control

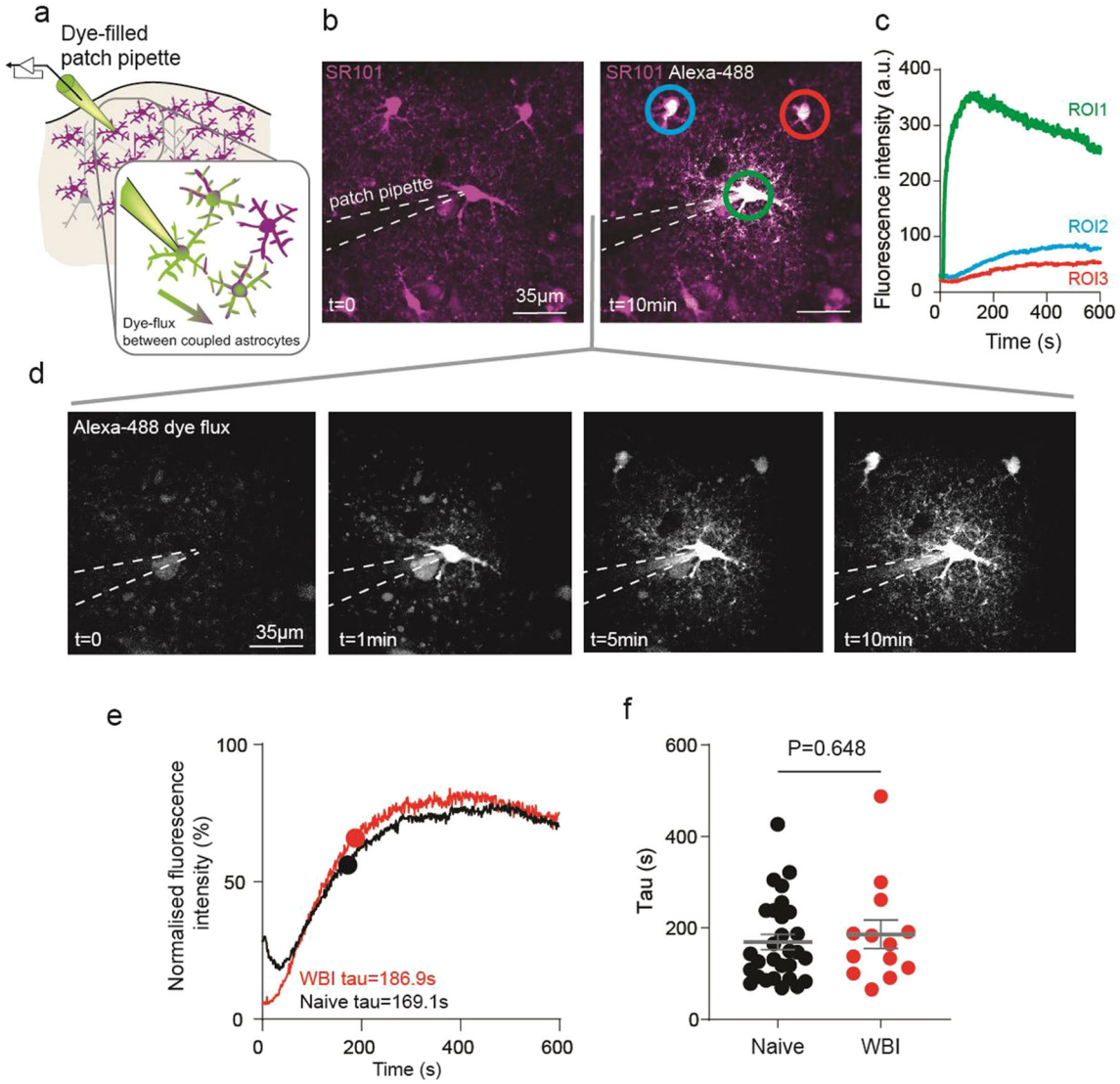

Fig. 2 Cortical astrocyte coupling is uncompromised after whole brain irradiation (WBI). **a** Schematic diagram of the experimental approach to investigate cortical astrocyte-to-astrocyte coupling using a dye-filled patch pipette which loads an astrocyte with a gap junction permeable dye. **b** Pseudocolored fluorescent 2-photon microscopy image of cortical astrocytes in layer 1 of the sensory-motor cortex preloaded with the astrocyte-specific structural dye sulforhodamine (SR) 101 (purple) before (left) and 10 min after (right) the patch pipette loaded the patched and neighboring astrocytes with Alexa-488-hydrazide (white). **c** Fluorescent intensity changes of Alexa-488-hydrazide in the patched astrocyte (region of interest (ROI) 1) and adjacent coupled astrocytes (ROI 2 and 3) over time. **d** The progression of Alexa-488-hydrazide flux (white) before ($t = 0$) and 1, 5, and 10 min after dye-loading started. **e** Normalized fluorescence intensity curve showing the mean trace of dye flux with the time constant (tau) of astrocytes from WBI (red) and from naive animals (black). **f** Tau values of dye filling kinetics showing the same coupling in naïve ($n = 29$ cells, 4 mice) and WBI ($n = 13$ cells, 4 mice) animals. $P = 0.648$, Mann–Whitney U test

directly apposed endfeet [19, 48]. To study WBI-induced changes in astrocytic Ca^{2+} signaling we used the Ca^{2+} indicator Rhod-2/AM, which bulk loads all neuronal and astrocytic cellular compartments [39]. Astrocytes exhibit brighter baseline fluorescence of Rhod-2, allowing to localize astrocyte soma and endfoot Ca^{2+} signals (Fig. 3b, f). Of note, using Rhod-2/AM, Ca^{2+} responses in fine processes of astrocytes cannot be spatially separated from Ca^{2+} changes in neuronal axons and dendrites; however, we previously reported that by using a combination of small-molecule or genetically encoded calcium indicators, neuron vs astrocyte Ca^{2+}

transients exhibit distinct onset times and kinetics in response to afferent stimulation, allowing us to distinguish between the different signals [39]. Here, the signal originating from neuronal and astrocyte processes combined is referred to as 'neuropil'.

A canonical pathway capable of increasing astrocyte free Ca^{2+} is the Gq-coupled α1 adrenergic receptor, which releases Ca^{2+} from intracellular stores. Cortical astrocytes are densely innervated by ascending noradrenergic fibers from the locus coeruleus, which upon activation produces large astrocyte Ca^{2+} transients associated with locomotion [49] or arousal [50–52]. This enhances astrocyte sensitivity to local circuit activity [49] and stimulates glycogenolysis to feed neurons with metabolic substrates [53]. The application of the selective α1-adrenergic receptor agonist phenylephrine (10 μM, in the superfused tissue bath) (Fig. 3a) evoked large Ca^{2+} increases in the neuropil which were identical in the WBI group ($\Delta F/F_{max} = 32 \pm 5\%$, $n = 11$ ROIs of 11 slices, 7 animals) to the control, sham-irradiated group ($\Delta F/F_{max} = 34 \pm 5\%$, $n = 7$ ROIs of 7 slices, 5 animals; $P = 0.857$, unpaired t test; Fig. 3b, c). Similarly, astrocyte somata developed the same Ca^{2+} response in the WBI group ($\Delta F/F_{max} = 187 \pm 27\%$, $n = 67$ cells averaged for 11 slices, 7 animals) as in the control group ($\Delta F/F_{max} = 159 \pm 9\%$, $n = 40$ cells averaged for 7 slices, 5 animals; $P = 0.228$, unpaired t test; Fig. 3d). These data indicate that α1-adrenergic receptor signaling is not impaired 12–15 months after WBI.

Another important stimulus to elicit astrocyte Ca^{2+} transients is the activation of glutamatergic synapses. We have previously shown that theta burst neural activity in neocortex causes enduring changes in synaptic strength [27] and generates large astrocyte Ca^{2+} signals that are sensitive to both ionotropic and metabotropic glutamate receptor inhibitors [38]. Such astrocytic Ca^{2+} signals are essential for regulation of synaptic plasticity related to learning and memory formation [54–56], and a failure of this mechanism could potentially contribute to postWBI cognitive decline, either through direct gliosynaptic effects, or indirect effects on synapses through impairments in vascular control. Therefore, we determined how WBI affected astrocyte Ca^{2+} responses related to glutamatergic synaptic activation using 30 s of theta burst electrical stimulation (Fig. 3e). Importantly, the region of cortical brain tissue imaged in our experiments had not only astrocytes and neurons, but also a penetrating blood vessel. This allowed us to quantify astrocyte Ca^{2+} signals in four primary compartments: somata, neuropil around an astrocyte soma, endfeet, and neuropil adjacent to the blood vessel (Fig. 3f).

In response to afferent stimulation using theta burst, we found that perivascular endfeet required higher voltage of stimulation to generate an endfoot Ca^{2+} increase in WBI brain slices (1.25 ± 0.04 V, $n = 9$ slices) than in control brain slices (1.1 ± 0.027 V, $n = 8$ slices, $p = 0.006$, Mann–Whitney U test), indicating reduced brain tissue excitability long after WBI treatment. We next measured periendfoot neuropil signals adjacent to the activated endfoot because it encompasses axons/dendrites and connected astrocyte processes that trigger endfoot Ca^{2+} transients upon activation (Fig. 3f). Neuronal elements and astrocyte processes exhibit different Ca^{2+} kinetics in response to electrical stimulation. We previously determined that neural process Ca^{2+} elevation is rapid (< 1 s), whereas astrocyte Ca^{2+} signals in brain slices appear 3 s following stimulation onset [39] (Fig. 3m). First, we quantified the early neuronal process Ca^{2+} peak in the periendfoot neuropil area and found no significant difference between the control ($\Delta F/F_{max} = 29 \pm 7\%$, $n = 8$ slices, 6 animals) and the WBI group ($\Delta F/F_{max} = 17 \pm 4\%$, $n = 9$ slices, 6 animals, $p = 0.12$, unpaired t test) (Fig. 3h). The overall neuropil Ca^{2+} peak (neural peak + astrocyte process Ca^{2+}) was also not different between sham-irradiated control ($\Delta F/F_{max} = 51 \pm 14\%$, $n = 8$ slices, 6 animals) and the WBI animals ($\Delta F/F_{max} = 33 \pm 6\%$, $n = 9$ slices, 6 animals; $p = 0.37$, Mann–Whitney U test; Fig. 3i). Importantly, stimulation-evoked astrocyte endfoot Ca^{2+} response curves were similar (Fig. 3j) and peak Ca^{2+} elevation was comparable in the WBI group ($\Delta F/F_{max} = 73 \pm 11\%$, $n = 9$ slices, 6 animal) to the sham-irradiated control group ($\Delta F/F_{max} = 99 \pm 17\%$, $n = 8$ slices, 6 animals; $p = 0.203$, Mann–Whitney U test; Fig. 3k).

We next evaluated the Ca^{2+} response of individual astrocyte somata within our field of view (200–300-μm across). The distance of each astrocyte relative to the position of the stimulating electrode was variable, so the activation of the surrounding brain tissue was heterogenous. This impacts the degree of each astrocyte's activation. In order to determine the synaptic activation surrounding astrocytes, we evaluated the neuropil Ca^{2+} response within a 25-μm radius around each astrocyte, termed "peri-astrocytic neuropil" (Fig. 3l), while avoiding cell bodies within this circle. We chose this size of region of interest, because we had previously quantified the area covered by the arbor of a single

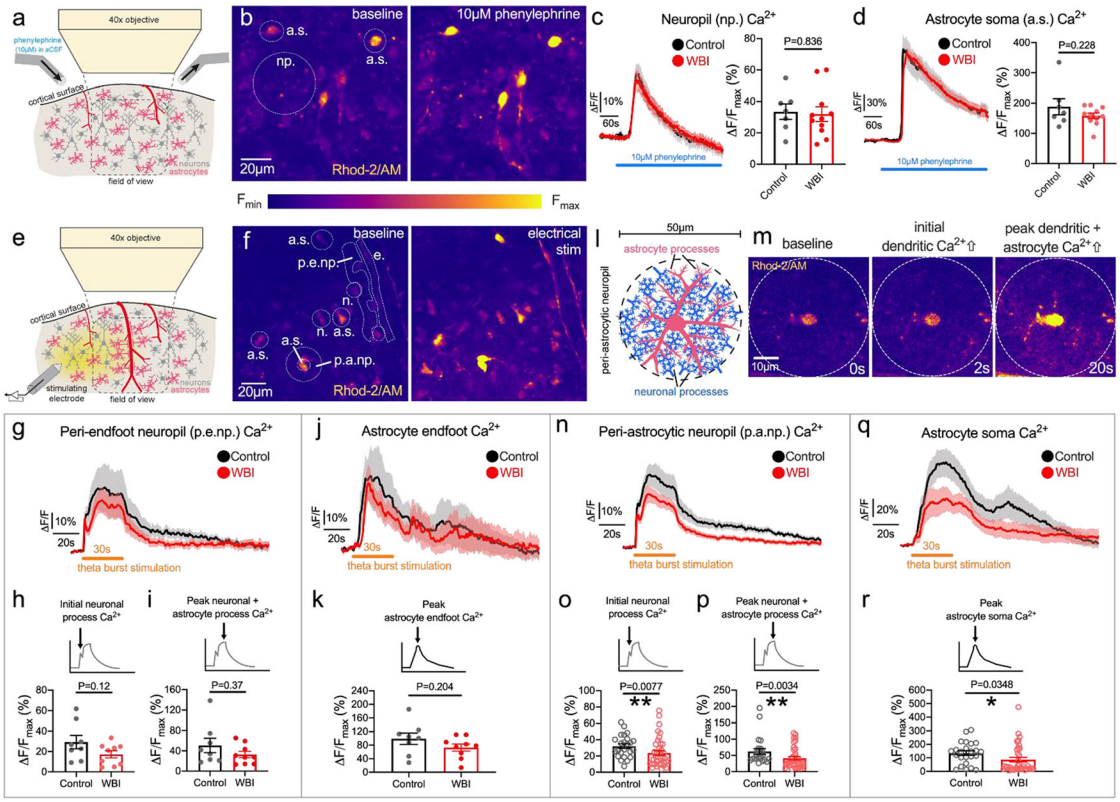

Fig. 3 Effects of whole brain irradiation (WBI) on cortical astrocyte Ca^{2+} responses to phenylephrine and to electrical stimulation. **a** Schematic diagram of the experimental setup to image cortical astrocyte Ca^{2+} responses to topical phenylephrine (10 μM) application with fluorescent 2-photon microscopy. **b** Pseudocolored fluorescent 2-photon microscopy image of cortical astrocytes in layers 1 and 2 of the sensory-motor cortex preloaded with the synthetic Ca^{2+} indicator Rhod-2/AM before and at the peak of phenylephrine-induced Ca^{2+} elevation. Np.: neuropil, a.s.: astrocyte soma. **c** Neuropil Ca^{2+} changes during 10-μM phenylephrine application and peak Ca^{2+} responses of control (7 ROIs of 7 slices, 5 mice) and WBI animals (11 ROIs of 11 slices, 7 mice). ROI: region of interest. **d** Astrocyte soma Ca^{2+} changes during 10-μM phenylephrine application and peak Ca^{2+} responses of Control (40 cells, 7 slices, 5 mice) and WBI animals (67 cells, 11 slices, 7 mice). ROI; region of interest. $\Delta F/F_{max}$: maximum relative fluorescence from 60 s baseline. Unpaired *t* test. $^{*}P < 0.05$. **e** Schematic diagram of the experimental setup to image cortical astrocyte Ca^{2+} responses to electrical stimulation with fluorescent 2-photon microscopy. **f** Pseudocolored fluorescent 2-photon microscopy image of cortical astrocytes in layers 1 and 2 of the sensory-motor cortex pre-loaded with the synthetic Ca^{2+} indicator Rhod-2/AM before (left image) and at the peak of electrical stimulation-evoked Ca^{2+} elevation (right image). A.s.: astrocyte soma, p.a.np.: peri-astrocytic neuropil, e: endfoot, p.e.np.: periendfoot neuropil, n: neuron soma. **g** Summary traces of the periendfoot neuropil Ca^{2+} changes during 30s theta burst stimulation in the WBI (red; 9 ROIs of 9 slices, 6 animals) and control (black; 8 ROIs of 8 slices, 6 animals) group (mean ± SEM). **h** Initial neuronal process Ca^{2+} response peak of the first 3 s of periendfoot neuropil Ca^{2+} elevation during 30 s theta burst stimulation (unpaired *t* test). **i** Peak neuronal process and astrocytic process Ca^{2+} elevation in the periendfoot neuropil in response to 30 s theta burst stimulation (Mann–Whitney *U* test). **j** Summary traces of astrocyte endfoot Ca^{2+} changes during 30 s theta burst stimulation in WBI (red; 9 ROIs of 9 slices, 6 mice) and Control (black; 8 ROIs of 8 slices, 6 mice) groups (mean ± SEM). **k** Endfoot Ca^{2+} transient peak elicited by 30 s theta burst stimulation (Mann–Whitney *U* test). **l** Schematic of the periastrocytic neuropil which contains astrocyte processes and neuronal processes. **m** Representative pseudocolored images of Rhod-2/AM fluorescence from an astrocyte and its periastrocytic neuropil area at baseline (0 s), 2 s, and 20 s after the onset of 30-s electrical stimulation. **n** Summary traces of the periastrocytic neuropil Ca^{2+} changes during 30-s theta burst stimulation in WBI (red; 38 ROIs, 9 slices, 6 animals) and in control mice (black; 24 ROIs, 8 slices, 6 animals) (mean ± SEM). **o** Peak of the initial neuronal process Ca^{2+} response during the first 3 s of periastrocytic neuropil Ca^{2+} elevation during 30 s theta burst stimulation (Mann–Whitney *U* test). **p** Peak neuronal process and astrocytic process Ca^{2+} elevation in the periastrocytic neuropil in response to 30 s theta burst stimulation (Mann–Whitney *U* test). **q** Summary traces of astrocyte soma Ca^{2+} changes during 30 s theta burst stimulation in WBI (red; 38 cells, 9 slices, 6 mice) and in control animals (black; 24 cells, 8 slices, 6 mice) (mean ± SEM). **r** Peak of astrocyte soma Ca^{2+} transients evoked by theta burst stimulation for 30 s in WBI (red) and control (black) groups (Mann–Whitney *U* test). $\Delta F/F_{max}$: maximum relative fluorescence increase from 10 s baseline. ROI: region of interest. $^{*}P < 0.05$, $^{**}P < 0.01$

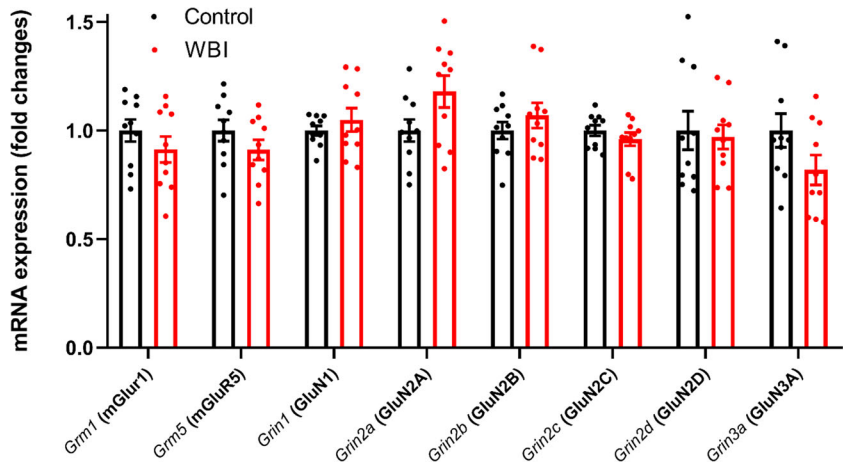

Fig. 4 Effects of whole brain irradiation (WBI) on cortical expression of glutamate receptors. qPCR data showing the mRNA expression of the group I metabotropic glutamate receptors Grm1 (mGluR1) and Grm5 (mGluR5) and the NMDAR subunits Grin1 (GluN1), Grin2a (GluN2A), Grin2b (GluN2B), Grin2c (GluN2C), Grin2d (GluN2D), and Grin3a (GluN3A) in cortical samples derived from WBI-treated ($n = 10$) and control ($n = 10$) mice. Differences were not significant by unpaired t test

astrocyte as ~2000 μm^2 [27]. The initial neuronal process Ca^{2+} peak in the periastrocytic neuropil of WBI astrocytes was significantly reduced ($\Delta F/F_{max} = 24 \pm 3\%$, $n = 38$ ROIs, 9 slices, 6 animals) from the initial peak response around control astrocytes ($\Delta F/F_{max} = 32 \pm 3\%$, $n = 24$ ROIs, 8 slices, 6 animals, $P = 0.0077$, Mann–Whitney U test; Fig. 3n, o). Likewise, the peak neuronal and astrocyte process Ca^{2+} signal of the WBI group ($\Delta F/F_{max} = 42 \pm 5\%$, $n = 38$ ROIs, 9 slices, 6 animals) was significantly less comparted to the control, sham-irradiated group ($\Delta F/F_{max} = 62 \pm 8\%$, $n = 24$ ROIs, 8 slices, 6 animals, $P = 0.0034$, Mann–Whitney U test; Fig. 3n, p). The peak astrocyte soma Ca^{2+} signal was also significantly compromised in WBI mice ($\Delta F/F_{max} = 87 \pm 17\%$, $n = 38$ cells, 9 slices, 6 animals) relative to control mice ($\Delta F/F_{max} = 135 \pm 17\%$, $n = 24$ cells, 8 slices, 6 animals, $P = 0.0348$, Mann–Whitney U test; Fig. 3q, r).

In order to verify that this significant difference in astrocyte soma Ca^{2+} was not a consequence of a higher or a lower synaptic activation in the periastrocytic neuropil across groups, we applied a generalized linear model using individual astrocyte soma Ca^{2+} peak values of WBI ($n = 38$ cells) and control slices ($n = 24$ cells), while including their corresponding initial neuronal process Ca^{2+} peak in the periastrocytic neuropil as a covariate. We found an overall significant effect of WBI ($P = 0.029$) on astrocyte soma Ca^{2+} peak, but no significant ($P = 0.119$) interaction between WBI and initial neuronal process Ca^{2+} peak, confirming that astrocytes of WBI animals are less responsive than astrocytes from control mice, irrespective of the differences in synaptic activation.

Effect of WBI on mRNA expression of glutamate receptors

Similar to neuronal cells, astrocytes express receptors for glutamate. Glutamate receptors that play a role in Ca^{2+} signaling and are expressed in astrocytes include metabotropic glutamate receptors (mGluR) [57] and ionotropic receptors N-methyl-D-aspartate receptors (NMDARs) [58]. The number of reactive [59–62] or senescent astrocytes [12] significantly increases 3–12 months after WBI, which could be accompanied by chronic changes in glutamate receptor expression. To determine whether WBI alters expression of glutamate receptors, we tested the mRNA expression of the group I metabotropic glutamate receptors Grm1 (mGluR1) and Grm5 (mGluR5) and the NMDAR subunits Grin1 (GluN1), Grin2a (GluN2A), Grin2b (GluN2B), Grin2c (GluN2C), Grin2d (GluN2D), and Grin3a (GluN3A) in cortical samples from WBI ($n = 5$) and sham-irradiated control mice ($n = 5$) 12 months after WBI, following behavioral testing by quantitative real time PCR (qPCR). However, we found that cortical expression of the glutamate receptor subunits studied was unaffected by WBI (unpaired t tests, all $P > 0.05$, Fig. 4). This suggests that the decrement in evoked astrocyte Ca^{2+}

signal we observed is unrelated to differences in glutamate receptor transcription.

Discussion

The key finding of this study is that late cognitive decline in mice induced by a clinical regimen of WBI is associated with persistent impairment of synaptic stimulation–induced astrocyte Ca^{2+} signaling. Previous in vivo and in vitro studies demonstrated that astrocytes are sensitive to γ-irradiation, which elicits persistent phenotypic and transcriptomic changes in them [12, 16]. Known γ-irradiation–induced changes in astrocytic phenotype include DNA damage response activation, transition to a presenescent state associated with chronic low-grade inflammation, alterations in the eicosanoid secretion profile and induction of cellular senescence, a permanent state of cell cycle arrest [12, 16]. This is the first study to demonstrate that the spectrum of irradiation-induced phenotypic changes in astrocytes also include persisting impairment of cellular Ca^{2+} signaling.

Genotoxic stress–related cellular phenotypic alterations may involve dysregulated expression of ion channels and altered function of cellular organelles, including the endoplasmic reticulum and the mitochondria, which play a key role in cellular Ca^{2+} handling. Previous studies showed that evoked Ca^{2+} signals in the astrocyte soma in response to theta burst activity is mediated by activation of ionotropic and metabotropic glutamate receptors and requires intact endoplasmic reticulum function, as it is absent if either glutamatergic signaling is inhibited or intracellular Ca^{2+} stores are depleted (e.g. by pretreatment with thapsigargin, a noncompetitive inhibitor of the sarco-/endoplasmic reticulum Ca^{2+} ATPase [SERCA]) [38]. It is also thought that the Ca^{2+} signal evoked by glutamate partially depends on the release of the gliotransmitter ATP triggered by activation of glutamate receptors. ATP is known to induce IP3-mediated release of Ca^{2+} from the endoplasmic reticulum as well as Ca^{2+} influx from the extracellular space, which mediate astrocytic Ca^{2+} waves [63]. We posit that the observed persisting changes in astrocyte Ca^{2+} responses related to glutamatergic synaptic activation may reflect altered glutamatergic or/and purinergic signaling, impaired production of ATP and/or WBI-related endoplasmic reticulum dysfunction. We cannot rule out that WBI also alters expression of astrocytic glutamate receptors, although their expression in cortical homogenates was unaltered. Heterogeneity in glutamatergic receptor density in various astrocyte compartments could underlie the differential impact of WBI on elicited soma and endfoot Ca^{2+} responses [64]. Alternatively, the decline in astrocyte soma Ca^{2+} signal elicited by electrical stimulation of theta burst pattern may indirectly reflect a shift of resting Ca^{2+} level. Accordingly, the size of evoked Ca^{2+} transients in astrocytes are inversely dictated by the resting concentration of free cytosolic Ca^{2+} [65]. Further, WBI is known to induce cellular senescence in astrocytes [12]. Senescent cells may exhibit altered Ca^{2+} homeostasis [66], thus it is possible that a causal link exists between astrocyte senescence and impaired astrocytic Ca^{2+} signaling. These hypotheses should be tested in future studies. Of note, the primary mechanism by which phenylephrine increases cytosolic Ca^{2+} is via IP3R2-mediated release from the ER [50], yet, this signaling pathway does not appear to be compromised by WBI. Impaired astrocyte Ca^{2+} signaling can disrupt astrocyte-to-neuron communication. As a consequence, synaptic dysfunction could progressively impair the ability of astrocytes to respond to synaptic activation. A plausible mechanism of attenuated Ca^{2+} transients in astrocytes, independent of astrocyte glutamate receptor expression, is reduced nitric oxide release from postsynaptic neurons [67–70]. We have previously demonstrated that selective inhibition of neuronal nitric oxide synthase completely prevents astrocyte soma Ca^{2+} transients to theta burst stimulation [38].

Astrocytic Ca^{2+} signaling is coupled to a wide range of downstream effector functions, including regulation of ion homeostasis, energy metabolism, gene expression, cell growth and cell division, and production/release of gliotransmitters and vasoactive mediators. There is increasing evidence suggesting that astrocytes, through signaling mechanisms controlled by Ca^{2+}, play a critical role in modulating neuronal activity and behavior [30] and regulate synaptic functions and plasticity via the release of gliotransmitters [71–77]. Similar to WBI, aging was found to decrease astrocyte Ca^{2+} signaling by glutamatergic stimulation, which diminishes the release of the gliotransmitter ATP from astrocytes, leading to a lower magnitude of LTP, the neuronal signature of memory [78–80]. Further studies are warranted to investigate how WBI-induced changes in astrocyte function [15] and Ca^{2+} signaling affect the aforementioned cellular functions and elucidate their contribution to the genesis of cognitive impairment.

Astrocytic Ca^{2+} signaling and astrocytic production of vasoactive mediators play an important role both in regulation of cerebral blood flow (CBF) and neurovascular coupling/functional hyperemia [21, 25, 81–83]. Recent studies show that in mice the same clinically relevant protocol of fractionated WBI that was used in the present study impairs astrocyte-mediated regulation of CBF [12]. This is a significant finding as impaired neurovascular coupling was shown to causally relate to cognitive decline [84–87]. Important astrocytic Ca^{2+}-regulated mechanisms that were suggested to contribute to CBF regulation and/or neurovascular coupling include production of arachidonic acid metabolites, including epoxygenase-derived epoxyeicosatrienoic acids (EETs) [88, 89] and cyclooxygenase-derived prostanoids [89–91] and/or release of ATP [92]. Astrocytic Ca^{2+} waves also release K^+ into the extracellular space through activation of BK_{Ca} channels [26, 82], which relax the arteriolar smooth muscle cells through activation of K_{IR} channels [93]. For more details pertaining the role of astrocyte Ca^{2+} signals in neurovascular coupling, see reviews [94–96]. Little is known about the vascular consequences to reduced astrocyte Ca^{2+} signals [97]. There is evidence that WBI alters the astrocytic production of vasodilator eicosanoid gliotransmitters [12], but its effect on cellular release of ATP and K^+ remains to be elucidated. Future studies should also determine how altered astrocytic Ca^{2+} signaling contributes to impaired CBF regulation and neurovascular dysfunction in WBI-treated animals.

Limitations of the study

There are important limitations of the study that should be considered. WBI was applied on 2-month-old, young-adult mice. Albeit cognitive impairment also develops in young, adult patients [98, 99], WBI is most commonly used in the aging population [100], and WBI of aging mice might trigger a different composition of astrocyte dysfunction than the findings of the current study, potentially due to changes in the WBI-evoked inflammatory response [101].

Rhod-2/AM does not detect astrocyte fine process microdomain Ca^{2+} transients. These microdomains generate Ca^{2+} signals independent of IP_3R2 in response to activation [50], perhaps through cell surface channels [102] or from mitochondrial Ca^{2+} stores [103]. Although sex hormones may affect cellular calcium signaling responses, we have not investigated sex-related differences in astrocyte Ca^{2+} responses in the present study. We have not systematically assessed changes in synaptic activity/excitability by WBI, which could have also contributed to astrocyte desensitization to glutamatergic activation. Further, we assessed changes in mRNA expression of glutamate receptors in bulk tissue. Abundant neuronal expression of these receptors may mask WBI-related expressional changes in astrocytes. Future studies using single cell transcriptomics may reveal distinct WBI-induced gene expression signatures in astrocytes. To assess WBI-induced changes in glutamate receptors at the protein level, immunostaining with a synaptic marker investigating colocalization would be informative.

Perspectives

In conclusion, our present and previous findings demonstrate that WBI results in persisting phenotypic and functional alterations in astrocytes, which include impairment of Ca^{2+} signaling responses. Exercise [104] or targeted reduction of inflammation [101, 105], oxidative stress [106, 107], and microglia activation [108] by miRNA-based, stem cell–derived extracellular vesicles [109] could potentially prevent WBI-related astrocyte dysfunction and cognitive impairment. Importantly, WBI was shown to induce cellular senescence in astrocytes, and depletion of senescent cells by genetic means or by treatment with the senolytic drug Navitoclax (ABT263) was demonstrated to rescue astrocytic neurovascular coupling responses in WBI-treated mice [12]. Thus, future studies should also determine how induction of cellular senescence by WBI affects astrocytic Ca^{2+} signaling responses and elucidate the effects of senolytic treatments. Postfixation detection of p16-driven expression of red fluorescent protein in brain slices derived from WBI-treated p16-3MR mice [12] used for Ca^{2+} signaling measurements would be informative in that regard.

Funding This work was supported by grants from the Oklahoma Center for the Advancement of Science and Technology, the National Institute on Aging (R01-AG047879; R01-AG055395), the National Institute of Neurological Disorders and Stroke (R01-NS056218, R01-NS100782), the Cellular and Molecular GeroScience CoBRE (P20GM125528) and the Canadian Institutes of Health Research, Foundation Grant (FDN-148471). G.R.G. was supported by Canada Research Chairs.

Compliance with ethical standards

Disclaimer The funding sources had no role in the study design; in the collection, analysis, and interpretation of data; in the writing of the report; and in the decision to submit the article for publication.

References

1. Gaspar LE, Mehta MP, Patchell RA, Burri SH, Robinson PD, Morris RE, et al. The role of whole brain radiation therapy in the management of newly diagnosed brain metastases: a systematic review and evidence-based clinical practice guideline. J Neuro-Oncol. 2010;96:17–32. https://doi.org/10.1007/s11060-009-0060-9.
2. Patil CG, Pricola K, Sarmiento JM, et al. Whole brain radiation therapy (WBRT) alone versus WBRT and radiosurgery for the treatment of brain metastases. Cochrane Database Syst Rev. 2017;9:CD006121. https://doi.org/10.1002/14651858.CD006121.pub4.
3. Lee YW, Cho HJ, Lee WH, Sonntag WE. Whole brain radiation-induced cognitive impairment: pathophysiological mechanisms and therapeutic targets. Biomol Ther (Seoul). 2012;20:357–70. https://doi.org/10.4062/biomolther.2012.20.4.357.
4. Khuntia D, Brown P, Li J, Mehta MP. Whole-brain radiotherapy in the management of brain metastasis. J Clin Oncol. 2006;24:1295–304. https://doi.org/10.1200/JCO.2005.04.6185.
5. Welzel G, Fleckenstein K, Schaefer J, Hermann B, Kraus-Tiefenbacher U, Mai SK, et al. Memory function before and after whole brain radiotherapy in patients with and without brain metastases. Int J Radiat Oncol Biol Phys. 2008;72:1311–8. https://doi.org/10.1016/j.ijrobp.2008.03.009.
6. Welzel G, Fleckenstein K, Mai SK, Hermann B, Kraus-Tiefenbacher U, Wenz F. Acute neurocognitive impairment during cranial radiation therapy in patients with intracranial tumors. Strahlenther Onkol. 2008;184:647–54. https://doi.org/10.1007/s00066-008-1830-6.
7. Vigliani MC, Duyckaerts C, Hauw JJ, Poisson M, Magdelenat H, Delattre JY. Dementia following treatment of brain tumors with radiotherapy administered alone or in combination with nitrosourea-based chemotherapy: a clinical and pathological study. J Neuro-Oncol. 1999;41:137–49. https://doi.org/10.1023/a:1006183730847.
8. Lamproglou I, Martin S, Diserbo M, et al. Total body 4.5 Gy gamma irradiation-induced early delayed learning and memory dysfunction in the rat. Cell Mol Biol (Noisy-le-grand). 2001;47:453–7.
9. Shi L, Adams MM, Long A, Carter CC, Bennett C, Sonntag WE, et al. Spatial learning and memory deficits after whole-brain irradiation are associated with changes in NMDA receptor subunits in the hippocampus. Radiat Res. 2006;166:892–9. https://doi.org/10.1667/RR0588.1.
10. Soussain C, Ricard D, Fike JR, Mazeron JJ, Psimaras D, Delattre JY. CNS complications of radiotherapy and chemotherapy. Lancet. 2009;374:1639–51. https://doi.org/10.1016/S0140-6736(09)61299-X.
11. Warrington JP, Csiszar A, Mitschelen M, Lee YW, Sonntag WE. Whole brain radiation-induced impairments in learning and memory are time-sensitive and reversible by systemic hypoxia. PLoS One. 2012;7:e30444. https://doi.org/10.1371/journal.pone.0030444.
12. Yabluchanskiy A, Tarantini S, Balasubramanian P, Kiss T, Csipo T, Fülöp GA, et al. Pharmacological or genetic depletion of senescent astrocytes prevents whole brain irradiation-induced impairment of neurovascular coupling responses protecting cognitive function in mice. Geroscience. 2020;133:446–28. https://doi.org/10.1007/s11357-020-00154-8.
13. Greene-Schloesser D, Robbins ME, Peiffer AM, Shaw EG, Wheeler KT, Chan MD. Radiation-induced brain injury: a review. Front Oncol. 2012;2:73. https://doi.org/10.3389/fonc.2012.00073.
14. Ungvari Z, Podlutsky A, Sosnowska D, Tucsek Z, Toth P, Deak F, et al. Ionizing radiation promotes the acquisition of a senescence-associated secretory phenotype and impairs angiogenic capacity in cerebromicrovascular endothelial cells: role of increased DNA damage and decreased DNA repair capacity in microvascular radiosensitivity. J Gerontol A Biol Sci Med Sci. 2013;68:1443–57. https://doi.org/10.1093/gerona/glt057.
15. Limbad C, Oron TR, Alimirah F, Davalos AR, Tracy TE, Gan L, et al. Astrocyte senescence promotes glutamate toxicity in cortical neurons. PLoS One. 2020;15:e0227887. https://doi.org/10.1371/journal.pone.0227887.
16. Turnquist C, Beck JA, Horikawa I, Obiorah IE, von Muhlinen N, Vojtesek B, et al. Radiation-induced astrocyte senescence is rescued by Δ133p53. Neuro-oncology. 2019;21:474–85. https://doi.org/10.1093/neuonc/noz001.
17. Cicciarello R, Russi E, Albiero F, Mesiti M, Torre E, D'Aquino A, et al. Cerebral metabolism and permeability of the hemato-encephalic barrier in an experimental model for brain radiotherapy. Radiol Med. 1990;80:709–12.
18. Buskila Y, Bellot-Saez A, Morley JW. Generating brain waves, the power of astrocytes. Front Neurosci. 2019;13:1125. https://doi.org/10.3389/fnins.2019.01125.
19. Gordon GRJ, Choi HB, Rungta RL, Ellis-Davies GCR, MacVicar BA. Brain metabolism dictates the polarity of astrocyte control over arterioles. Nature. 2008;456:745–9. https://doi.org/10.1038/nature07525.
20. Gordon GRJ, Howarth C, MacVicar BA. Bidirectional control of arteriole diameter by astrocytes. Exp Physiol. 2011;96:393–9. https://doi.org/10.1113/expphysiol.2010.053132.
21. Gordon GRJ, Mulligan SJ, MacVicar BA. Astrocyte control of the cerebrovasculature. Glia. 2007;55:1214–21. https://doi.org/10.1002/glia.20543.
22. Filosa JA, Morrison HW, Iddings JA, du W, Kim KJ. Beyond neurovascular coupling, role of astrocytes in the regulation of vascular tone. Neuroscience. 2016;323:96–109. https://doi.org/10.1016/j.neuroscience.2015.03.064.
23. Otsu Y, Couchman K, Lyons DG, Collot M, Agarwal A, Mallet JM, et al. Calcium dynamics in astrocyte processes during neurovascular coupling. Nat Neurosci. 2015;18:210–8. https://doi.org/10.1038/nn.3906.

24. Petzold GC, Murthy VN. Role of astrocytes in neurovascular coupling. Neuron. 2011;71:782–97. https://doi.org/10.1016/j.neuron.2011.08.009.
25. Filosa JA, Bonev AD, Nelson MT. Calcium dynamics in cortical astrocytes and arterioles during neurovascular coupling. Circ Res. 2004;95:e73–81. https://doi.org/10.1161/01.RES.0000148636.60732.2e.
26. Girouard H, Bonev AD, Hannah RM, Meredith A, Aldrich RW, Nelson MT. Astrocytic endfoot Ca2+ and BK channels determine both arteriolar dilation and constriction. Proc Natl Acad Sci U S A. 2010;107:3811–6. https://doi.org/10.1073/pnas.0914722107.
27. Murphy-Royal C, Johnston AD, Boyce AKJ, Diaz-Castro B, Institoris A, Peringod G, et al. Stress gates an astrocytic energy reservoir to impair synaptic plasticity. Nat Commun. 2020;11:2014–8. https://doi.org/10.1038/s41467-020-15778-9.
28. Vincent AJ, Gasperini R, Foa L, Small DH. Astrocytes in Alzheimer's disease: emerging roles in calcium dysregulation and synaptic plasticity. J Alzheimers Dis. 2010;22:699–714. https://doi.org/10.3233/JAD-2010-101089.
29. Yu X, Taylor AMW, Nagai J, et al. Reducing astrocyte calcium signaling in vivo alters striatal microcircuits and causes repetitive behavior. Neuron. 2018;99:1170–1187.e9. https://doi.org/10.1016/j.neuron.2018.08.015.
30. Cao X, Li L-P, Wang Q, Wu Q, Hu HH, Zhang M, et al. Astrocyte-derived ATP modulates depressive-like behaviors. Nat Med. 2013;19:773–7. https://doi.org/10.1038/nm.3162.
31. Padmashri R, Suresh A, Boska MD, Dunaevsky A. Motor-skill learning is dependent on astrocytic activity. Neural Plast. 2015;2015:938023–11. https://doi.org/10.1155/2015/938023.
32. Claro S, Oshiro MEM, Freymuller E, Katchburian E, Kallas EG, Cerri PS, et al. Gamma-radiation induces apoptosis via sarcoplasmatic reticulum in guinea pig ileum smooth muscle cells. Eur J Pharmacol. 2008;590:20–8. https://doi.org/10.1016/j.ejphar.2008.05.038.
33. Chatterjee J, Nairy RK, Langhnoja J, Tripathi A, Patil RK, Pillai PP, et al. ER stress and genomic instability induced by gamma radiation in mice primary cultured glial cells. Metab Brain Dis. 2018;33:855–68. https://doi.org/10.1007/s11011-018-0183-9.
34. Kandasamy SB, Howerton TC, Hunt WA. Reductions in calcium uptake induced in rat brain synaptosomes by ionizing radiation. Radiat Res. 1991;125:158–62.
35. Demaria M, Ohtani N, Youssef SA, Rodier F, Toussaint W, Mitchell JR, et al. An essential role for senescent cells in optimal wound healing through secretion of PDGF-AA. Dev Cell. 2014;31:722–33. https://doi.org/10.1016/j.devcel.2014.11.012.
36. Demaria M, O'Leary MN, Chang J, Shao L, Liu S, Alimirah F, et al. Cellular senescence promotes adverse effects of chemotherapy and cancer relapse. Cancer Discov. 2017;7:165–76. https://doi.org/10.1158/2159-8290.CD-16-0241.
37. Warrington JP, Csiszar A, Johnson DA, Herman TS, Ahmad S, Lee YW, et al. Cerebral microvascular rarefaction induced by whole brain radiation is reversible by systemic hypoxia in mice. Am J Physiol Heart Circ Physiol. 2011;300:H736–44. https://doi.org/10.1152/ajpheart.01024.2010.
38. Mehina EMF, Murphy-Royal C, Gordon GR. Steady-state free Ca2+ in astrocytes is decreased by experience and impacts arteriole tone. J Neurosci. 2017;37:8150–65. https://doi.org/10.1523/JNEUROSCI.0239-17.2017.
39. Institoris A, Rosenegger DG, Gordon GR. Arteriole dilation to synaptic activation that is sub-threshold to astrocyte endfoot Ca2+ transients. J Cereb Blood Flow Metab. 2015;35:1411–5. https://doi.org/10.1038/jcbfm.2015.141.
40. Rosenegger DG, Tran CHT, LeDue J, Zhou N, Gordon GR. A high performance, cost-effective, open-source microscope for scanning two-photon microscopy that is modular and readily adaptable. PLoS One. 2014;9:e110475. https://doi.org/10.1371/journal.pone.0110475.
41. Hess G, Donoghue JP. Long-term potentiation of horizontal connections provides a mechanism to reorganize cortical motor maps. J Neurophysiol. 1994;71:2543–7. https://doi.org/10.1152/jn.1994.71.6.2543.
42. Castro-Alamancos MA, Donoghue JP, Connors BW. Different forms of synaptic plasticity in somatosensory and motor areas of the neocortex. J Neurosci. 1995;15:5324–33.
43. Collins GG. The characteristics and pharmacology of olfactory cortical LTP induced by theta-burst high frequency stimulation and 1S,3R-ACPD. Neuropharmacology. 1994;33:87–95. https://doi.org/10.1016/0028-3908(94)90101-5.
44. Pannasch U, Vargová L, Reingruber J, et al. Astroglial networks scale synaptic activity and plasticity. Proc Natl Acad Sci U S A. 2011;108:8467–72. https://doi.org/10.1073/pnas.1016650108.
45. Beckner ME. A roadmap for potassium buffering/dispersion via the glial network of the CNS. Neurochem Int. 2020;136:104727. https://doi.org/10.1016/j.neuint.2020.104727.
46. Deemyad T, Lüthi J, Spruston N. Astrocytes integrate and drive action potential firing in inhibitory subnetworks. Nat Commun. 2018;9:4336. https://doi.org/10.1038/s41467-018-06338-3.
47. Boison D, Steinhäuser C. Epilepsy and astrocyte energy metabolism. Glia. 2018;66:1235–43. https://doi.org/10.1002/glia.23247.
48. Mulligan SJ, MacVicar BA. Calcium transients in astrocyte endfeet cause cerebrovascular constrictions. Nature. 2004;431:195–9. https://doi.org/10.1038/nature02827.
49. Paukert M, Agarwal A, Cha J, Doze VA, Kang JU, Bergles DE. Norepinephrine controls astroglial responsiveness to local circuit activity. Neuron. 2014;82:1263–70. https://doi.org/10.1016/j.neuron.2014.04.038.
50. Srinivasan R, Huang BS, Venugopal S, Johnston AD, Chai H, Zeng H, et al. Ca(2+) signaling in astrocytes from Ip3r2(−/−) mice in brain slices and during startle responses in vivo. Nat Neurosci. 2015;18:708–17. https://doi.org/10.1038/nn.4001.
51. Bonder DE, McCarthy KD. Astrocytic Gq-GPCR-linked IP3R-dependent Ca2+ signaling does not mediate neurovascular coupling in mouse visual cortex in vivo. J Neurosci. 2014;34:13139–50. https://doi.org/10.1523/JNEUROSCI.2591-14.2014.

52. Bekar LK, He W, Nedergaard M. Locus coeruleus alpha-adrenergic-mediated activation of cortical astrocytes in vivo. Cereb Cortex. 2008;18:2789–95. https://doi.org/10.1093/cercor/bhn040.
53. Magistretti PJ, Allaman I. A cellular perspective on brain energy metabolism and functional imaging. Neuron. 2015;86:883–901. https://doi.org/10.1016/j.neuron.2015.03.035.
54. Mothet J-P, Pollegioni L, Ouanounou G, Martineau M, Fossier P, Baux G. Glutamate receptor activation triggers a calcium-dependent and SNARE protein-dependent release of the gliotransmitter D-serine. Proc Natl Acad Sci U S A. 2005;102:5606–11. https://doi.org/10.1073/pnas.0408483102.
55. Parpura V, Basarsky TA, Liu F, Jeftinija K, Jeftinija S, Haydon PG. Glutamate-mediated astrocyte-neuron signalling. Nature. 1994;369:744–7. https://doi.org/10.1038/369744a0.
56. Panatier A, Theodosis DT, Mothet J-P, Touquet B, Pollegioni L, Poulain DA, et al. Glia-derived D-serine controls NMDA receptor activity and synaptic memory. Cell. 2006;125:775–84. https://doi.org/10.1016/j.cell.2006.02.051.
57. Spampinato SF, Copani A, Nicoletti F, Sortino MA, Caraci F. Metabotropic glutamate receptors in glial cells: a new potential target for neuroprotection? Front Mol Neurosci. 2018;11:414. https://doi.org/10.3389/fnmol.2018.00414.
58. Skowrońska K, Obara-Michlewska M, Zielińska M, Albrecht J. NMDA receptors in astrocytes: in search for roles in neurotransmission and astrocytic homeostasis. Int J Mol Sci. 2019;20:309. https://doi.org/10.3390/ijms20020309.
59. Chiang CS, McBride WH, Withers HR. Radiation-induced astrocytic and microglial responses in mouse brain. Radiother Oncol. 1993;29:60–8. https://doi.org/10.1016/0167-8140(93)90174-7.
60. Suman S, Rodriguez OC, Winters TA, et al. Therapeutic and space radiation exposure of mouse brain causes impaired DNA repair response and premature senescence by chronic oxidant production. Aging (Albany NY). 2013;5:607–22. https://doi.org/10.18632/aging.100587.
61. Bálentová S, Hnilicová P, Kalenská D, Murín P, Hajtmanová E, Lehotský J, et al. Effect of whole-brain irradiation on the specific brain regions in a rat model: metabolic and histopathological changes. Neurotoxicology. 2017;60:70–81. https://doi.org/10.1016/j.neuro.2017.03.005.
62. Bálentová S, Hajtmanová E, Filová B, Borbélyová V, Lehotský J, Adamkov M. Effects of fractionated whole-brain irradiation on cellular composition and cognitive function in the rat brain. Int J Radiat Biol. 2018;94:238–47. https://doi.org/10.1080/09553002.2018.1425805.
63. Verkhratsky A, Nedergaard M. Physiology of astroglia. Physiol Rev. 2018;98:239–389. https://doi.org/10.1152/physrev.00042.2016.
64. Panatier A, Vallée J, Haber M, Murai KK, Lacaille JC, Robitaille R. Astrocytes are endogenous regulators of basal transmission at central synapses. Cell. 2011;146:785–98. https://doi.org/10.1016/j.cell.2011.07.022.
65. King CM, Bohmbach K, Minge D, et al. Local resting Ca2+ controls the scale of astroglial Ca2+ signals. Cell Rep. 2020;30:3466–3477.e4. https://doi.org/10.1016/j.celrep.2020.02.043.
66. Janikiewicz J, Szymański J, Malinska D, Patalas-Krawczyk P, Michalska B, Duszyński J, et al. Mitochondria-associated membranes in aging and senescence: structure, function, and dynamics. Cell Death Dis. 2018;9:332. https://doi.org/10.1038/s41419-017-0105-5.
67. Bal-Price A, Moneer Z, Brown GC. Nitric oxide induces rapid, calcium-dependent release of vesicular glutamate and ATP from cultured rat astrocytes. Glia. 2002;40:312–23. https://doi.org/10.1002/glia.10124.
68. Li N, Sul J-Y, Haydon PG. A calcium-induced calcium influx factor, nitric oxide, modulates the refilling of calcium stores in astrocytes. J Neurosci. 2003;23:10302–10. https://doi.org/10.1523/JNEUROSCI.23-32-10302.2003.
69. Schipke CG, Heidemann A, Skupin A, Peters O, Falcke M, Kettenmann H. Temperature and nitric oxide control spontaneous calcium transients in astrocytes. Cell Calcium. 2008;43:285–95. https://doi.org/10.1016/j.ceca.2007.06.002.
70. Brenman JE, Christopherson KS, Craven SE, McGee AW, Bredt DS. Cloning and characterization of postsynaptic density 93, a nitric oxide synthase interacting protein. J Neurosci. 1996;16:7407–15. https://doi.org/10.1523/JNEUROSCI.16-23-07407.1996.
71. Sasaki T, Ishikawa T, Abe R, Nakayama R, Asada A, Matsuki N, et al. Astrocyte calcium signalling orchestrates neuronal synchronization in organotypic hippocampal slices. J Physiol Lond. 2014;592:2771–83. https://doi.org/10.1113/jphysiol.2014.272864.
72. Araque A. Astrocytes process synaptic information. Neuron Glia Biol. 2008;4:3–10. https://doi.org/10.1017/S1740925X09000064.
73. Kofuji P, Araque A. G-protein-coupled receptors in astrocyte-neuron communication. Neuroscience. 2020. https://doi.org/10.1016/j.neuroscience.2020.03.025.
74. Navarrete M, Perea G, Maglio L, Pastor J, Garcia de Sola R, Araque A. Astrocyte calcium signal and gliotransmission in human brain tissue. Cereb Cortex. 2013;23:1240–6. https://doi.org/10.1093/cercor/bhs122.
75. Perea G, Araque A. GLIA modulates synaptic transmission. Brain Res Rev. 2010;63:93–102. https://doi.org/10.1016/j.brainresrev.2009.10.005.
76. Henneberger C, Papouin T, Oliet SHR, Rusakov DA. Long-term potentiation depends on release of D-serine from astrocytes. Nature. 2010;463:232–6. https://doi.org/10.1038/nature08673.
77. Pascual O, Casper KB, Kubera C, et al. Astrocytic purinergic signaling coordinates synaptic networks. Science. 2005;310:113–6. https://doi.org/10.1126/science.1116916.
78. Gómez-Gonzalo M, Martin-Fernandez M, Martínez-Murillo R, Mederos S, Hernández-Vivanco A, Jamison S, et al. Neuron-astrocyte signaling is preserved in the aging brain. Glia. 2017;65:569–80. https://doi.org/10.1002/glia.23112.
79. Lalo U, Rasooli-Nejad S, Pankratov Y. Exocytosis of gliotransmitters from cortical astrocytes: implications for synaptic plasticity and aging. Biochem Soc Trans. 2014;42:1275–81. https://doi.org/10.1042/BST20140163.

80. Lalo U, Palygin O, North RA, Verkhratsky A, Pankratov Y. Age-dependent remodelling of ionotropic signalling in cortical astroglia. Aging Cell. 2011;10:392–402. https://doi.org/10.1111/j.1474-9726.2011.00682.x.
81. Dunn KM, Hill-Eubanks DC, Liedtke WB, Nelson MT. TRPV4 channels stimulate Ca2+-induced Ca2+ release in astrocytic endfeet and amplify neurovascular coupling responses. Proc Natl Acad Sci U S A. 2013;110:6157–62. https://doi.org/10.1073/pnas.1216514110.
82. Longden TA, Dunn KM, Draheim HJ, Nelson MT, Weston AH, Edwards G. Intermediate-conductance calcium-activated potassium channels participate in neurovascular coupling. Br J Pharmacol. 2011;164:922–33. https://doi.org/10.1111/j.1476-5381.2011.01447.x.
83. Straub SV, Bonev AD, Wilkerson MK, Nelson MT. Dynamic inositol trisphosphate-mediated calcium signals within astrocytic endfeet underlie vasodilation of cerebral arterioles. J Gen Physiol. 2006;128:659–69. https://doi.org/10.1085/jgp.200609650.
84. Tarantini S, Hertelendy P, Tucsek Z, Valcarcel-Ares MN, Smith N, Menyhart A, et al. Pharmacologically-induced neurovascular uncoupling is associated with cognitive impairment in mice. J Cereb Blood Flow Metab. 2015;35:1871–81. https://doi.org/10.1038/jcbfm.2015.162.
85. Tarantini S, Valcarcel-Ares MN, Toth P, Yabluchanskiy A, Tucsek Z, Kiss T, et al. Nicotinamide mononucleotide (NMN) supplementation rescues cerebromicrovascular endothelial function and neurovascular coupling responses and improves cognitive function in aged mice. Redox Biol. 2019;24:101192. https://doi.org/10.1016/j.redox.2019.101192.
86. Tarantini S, Valcarcel-Ares NM, Yabluchanskiy A, Fulop GA, Hertelendy P, Gautam T, et al. Treatment with the mitochondrial-targeted antioxidant peptide SS-31 rescues neurovascular coupling responses and cerebrovascular endothelial function and improves cognition in aged mice. Aging Cell. 2018;17:e12731. https://doi.org/10.1111/acel.12731.
87. Tarantini S, Valcarcel-Ares MN, Yabluchanskiy A, Tucsek Z, Hertelendy P, Kiss T, et al. Nrf2 deficiency exacerbates obesity-induced oxidative stress, neurovascular dysfunction, blood-brain barrier disruption, neuroinflammation, amyloidogenic gene expression, and cognitive decline in mice, mimicking the aging phenotype. J Gerontol A Biol Sci Med Sci. 2018;73:853–63. https://doi.org/10.1093/gerona/glx177.
88. Attwell D, Buchan AM, Charpak S, Lauritzen M, MacVicar BA, Newman EA. Glial and neuronal control of brain blood flow. Nature. 2010;468:232–43. https://doi.org/10.1038/nature09613.
89. Toth P, Tarantini S, Ashpole NM, Tucsek Z, Milne GL, Valcarcel-Ares NM, et al. IGF-1 deficiency impairs neurovascular coupling in mice: implications for cerebromicrovascular aging. Aging Cell. 2015;14:1034–44. https://doi.org/10.1111/acel.12372.
90. Rosenegger DG, Tran CHT, Wamsteeker Cusulin JI, Gordon GR. Tonic local brain blood flow control by astrocytes independent of phasic neurovascular coupling. J Neurosci. 2015;35:13463–74. https://doi.org/10.1523/JNEUROSCI.1780-15.2015.
91. Czigler A, Toth L, Szarka N, Szilágyi K, Kellermayer Z, Harci A, et al. Prostaglandin E2, a postulated mediator of neurovascular coupling, at low concentrations dilates whereas at higher concentrations constricts human cerebral parenchymal arterioles. Prostaglandins Other Lipid Mediat. 2020;146:106389. https://doi.org/10.1016/j.prostaglandins.2019.106389.
92. Toth P, Tarantini S, Davila A, Valcarcel-Ares MN, Tucsek Z, Varamini B, et al. Purinergic glio-endothelial coupling during neuronal activity: role of P2Y1 receptors and eNOS in functional hyperemia in the mouse somatosensory cortex. Am J Physiol Heart Circ Physiol. 2015;309:H1837–45. https://doi.org/10.1152/ajpheart.00463.2015.
93. Dunn KM, Nelson MT. Potassium channels and neurovascular coupling. Circ J. 2010;74:608–16. https://doi.org/10.1253/circj.cj-10-0174.
94. Tarantini S, Tran CHT, Gordon GR, Ungvari Z, Csiszar A. Impaired neurovascular coupling in aging and Alzheimer's disease: contribution of astrocyte dysfunction and endothelial impairment to cognitive decline. Exp Gerontol. 2017;94:52–8. https://doi.org/10.1016/j.exger.2016.11.004.
95. Bazargani N, Attwell D. Astrocyte calcium signaling: the third wave. Nat Neurosci. 2016;19:182–9. https://doi.org/10.1038/nn.4201.
96. Iadecola C. The neurovascular unit coming of age: a journey through neurovascular coupling in health and disease. Neuron. 2017;96:17–42. https://doi.org/10.1016/j.neuron.2017.07.030.
97. Verkhratsky A. Astroglial calcium signaling in aging and Alzheimer's disease. Cold Spring Harb Perspect Biol. 2019;11:a035188. https://doi.org/10.1101/cshperspect.a035188.
98. Morrison MA, Mueller S, Felton E, Jakary A, Stoller S, Avadiappan S, et al. Rate of radiation-induced microbleed formation on 7T MRI relates to cognitive impairment in young patients treated with radiation therapy for a brain tumor. Radiother Oncol. 2020;154:145–53. https://doi.org/10.1016/j.radonc.2020.09.028.
99. Agbahiwe H, Rashid A, Horska A, Mahone EM, Lin D, McNutt T, et al. A prospective study of cerebral, frontal lobe, and temporal lobe volumes and neuropsychological performance in children with primary brain tumors treated with cranial radiation. Cancer. 2017;123:161–8. https://doi.org/10.1002/cncr.30313.
100. Chan S, Rowbottom L, McDonald R, et al. Could time of whole brain radiotherapy delivery impact overall survival in patients with multiple brain metastases? Ann Palliat Med. 2016;5:267–79. https://doi.org/10.21037/apm.2016.09.05.
101. Lee WH, Sonntag WE, Lee YW. Aging attenuates radiation-induced expression of pro-inflammatory mediators in rat brain. Neurosci Lett. 2010;476:89–93. https://doi.org/10.1016/j.neulet.2010.04.009.
102. Rungta RL, Bernier L-P, Dissing-Olesen L, Groten CJ, LeDue JM, Ko R, et al. Ca2+ transients in astrocyte fine processes occur via Ca2+ influx in the adult mouse hippocampus. Glia. 2016;64:2093–103. https://doi.org/10.1002/glia.23042.
103. Agarwal A, Wu P-H, Hughes EG, et al. Transient opening of the mitochondrial permeability transition pore induces

microdomain calcium transients in astrocyte processes. Neuron. 2017;93:587–605.e7. https://doi.org/10.1016/j.neuron.2016.12.034.

104. Wong-Goodrich SJE, Pfau ML, Flores CT, Fraser JA, Williams CL, Jones LW. Voluntary running prevents progressive memory decline and increases adult hippocampal neurogenesis and growth factor expression after whole-brain irradiation. Cancer Res. 2010;70:9329–38. https://doi.org/10.1158/0008-5472.CAN-10-1854.
105. Lee WH, Sonntag WE, Mitschelen M, Yan H, Lee YW. Irradiation induces regionally specific alterations in pro-inflammatory environments in rat brain. Int J Radiat Biol. 2010;86:132–44. https://doi.org/10.3109/09553000903419346.
106. Banerjee S, Aykin-Burns N, Krager KJ, Shah SK, Melnyk SB, Hauer-Jensen M, et al. Loss of C/EBPδ enhances IR-induced cell death by promoting oxidative stress and mitochondrial dysfunction. Free Radic Biol Med. 2016;99:296–307. https://doi.org/10.1016/j.freeradbiomed.2016.08.022.
107. Jou M-J. Pathophysiological and pharmacological implications of mitochondria-targeted reactive oxygen species generation in astrocytes. Adv Drug Deliv Rev. 2008;60:1512–26. https://doi.org/10.1016/j.addr.2008.06.004.
108. Allen BD, Syage AR, Maroso M, Baddour AAD, Luong V, Minasyan H, et al. Mitigation of helium irradiation-induced brain injury by microglia depletion. J Neuroinflammation. 2020;17:159. https://doi.org/10.1186/s12974-020-01790-9.
109. Leavitt RJ, Limoli CL, Baulch JE. miRNA-based therapeutic potential of stem cell-derived extracellular vesicles: a safe cell-free treatment to ameliorate radiation-induced brain injury. Int J Radiat Biol. 2019;95:427–35. https://doi.org/10.1080/09553002.2018.1522012.